Stability of Polydimethylsiloxane−Magnetite Nanoparticle Dispersions Against Flocculation: Interparticle Interactions of Polydisperse Materials

ARTICLE *in* LANGMUIR · JUNE 2008

Impact Factor: 4.46 · DOI: 10.1021/la703146y · Source: PubMed

Stability of Polydimethylsiloxane-Magnetite Nanoparticle Dispersions Against Flocculation: Interparticle Interactions of Polydisperse Materials

O. Thompson Mefford,[†] Michael L. Vadala,[‡] Jonathan D. Goff,[†] Matthew R. J. Carroll,[§] Raquel Mejia-Ariza,[†] Beth L. Caba,[†] Timothy G. St. Pierre,[§] Robert C. Woodward,[§] Richey M. Davis,[†] and J. S. Riffle*[,†]

Macromolecules and Interfaces Institute, Virginia Tech, Blacksburg, Virginia 24061, NanoMedics, LLC, Erie, Pennsylvania 16505, and School of Physics, University of Western Australia, Crawley, Western Australia 6009, Australia

Received October 10, 2007. In Final Form: February 11, 2008

The colloidal stability of dispersions comprised of magnetite nanoparticles coated with polydimethylsiloxane (PDMS) oligomers was investigated theoretically and experimentally. Particle−particle interaction potentials in a theta solvent and in a good solvent for the PDMS were predicted by calculating van der Waals, electrostatic, steric, and magnetic forces as functions of interparticle separation distances. A variety of nanoparticle sizes and size distributions were considered. Calculations of the interparticle potential in dilute suspensions indicated that flocculation was likely for the largest 1% of the population of particles. Finally, the rheology of these complexes over time in the absence of a solvent was measured to probe their stabilities against flocculation as neat fluids. An increase in viscosity was observed upon aging, suggesting that some agglomeration occurs with time. However, the effects of aging could be removed by exposing the sample to high shear, indicating that the magnetic fluids were not irreversibly flocculated.

Introduction

In recent years, the use of magnetic nanoparticles in medical applications has grown significantly. Currently, magnetic nanoparticles are utilized as contrast agents for MRI to diagnose tumors and cardiovascular disease, as hyperthermia agents for brain cancer therapy, and for magnetic separations of cells and bioagents.[1−5] In addition, researchers in our laboratories have synthesized hydrophobic ferrofluids comprised of polymer-coated magnetite nanoparticles for treating retinal detachments.[6−11] These latter materials are the focus of this paper.

Tailoring the surfaces of these materials is critical for the success of these applications. Polymers that form sheaths around the magnetic nanoparticles can function to (i) suspend the nanoparticles in the intended medium, (ii) provide a stabilizing layer that prevents agglomeration, and (iii) reduce immune response. This has been accomplished with a variety of polymers.[12] For example, magnetic iron oxide particles have been coated with homopolymers such as poly(acrylic acid),[13] random copolymers such as poly(oligo(ethylene oxide) methacrylate-*co*-methacrylic acid),[14] or block copolymers such as poly(ethylene oxide-*block*-methacrylic acid).[15] In addition, iron oxide nanoparticles have been coated with water soluble polymers such as dextran[16] and poly(ethylene oxide)[3,17,18] and with nonpolar materials such as polystyrene and poly(methyl methacrylate).[19]

The stabilities of polymer-magnetite complexes in dilute suspensions are related to the net particle−particle interaction potentials. Particles are attracted by van der Waals and magnetic interactions and repelled by steric and electrostatic forces. To maintain stability of a dispersion, the repulsive forces must be substantial enough to prevent agglomeration driven by the attractive forces. This balance has been extensively studied in the realm of colloidal suspensions. The classical approach utilizes Derjaguin−Landau−Verwey−Overbeek (DLVO) theory[20−23] as

* Corresponding author. E-mail: JudyRiffle@aol.com. Phone: (540)-231-8214.

[†] Virginia Tech.

[‡] NanoMedics, LLC.

[§] University of Western Australia.

(1) Willard, M. A.; Kurihara, L. K.; Carpenter, E. E.; Calvin, S.; Harris, V. G. *Int. Mater. Rev.* **2004**, *49* (3−4), 125−170.

(2) Neuberger, T.; Schopf, B.; Hofmann, H.; Hofmann, M.; von Rechenberg, B. *J. Magn. Magn. Mater.* **2005**, *293* (1), 483−496.

(3) Thunemann, A. F.; Schutt, D.; Kaufner, L.; Pison, U.; Mohwald, H. *Langmuir* **2006**, *22*, 2351−2357.

(4) Pankhurst, Q. A.; Connolly, J.; Jones, S. K.; Dobson, J. *J. Phys. D: Appl. Phys.* **2003**, *36*, R167−181.

(5) Tartaj, P.; Puerto-Morales, M. D.; Veintemillas-Verdaguer, S.; Gonzalez-Carreno, T.; Serna, C. J. *J. Phys. D: Appl. Phys.* **2003**, *36*, R182−R197.

(6) Dailey, J. P.; Phillips, J. P.; Li, C.; Riffle, J. S. *J. Magn. Magn. Mater.* **1999**, *194*, 140−148.

(7) Mefford, O. T.; Woodward, R. C.; Goff, J. D.; Vadala, T. P.; St. Pierre, T. G.; Dailey, J. P.; Riffle, J. S. *J. Magn. Magn. Mater.* **2007**, *311*, 347−353.

(8) Rutnakornpituk, M.; Baranauskas, V. V.; Riffle, J. S.; Connolly, J.; St. Pierre, T. G.; Dailey, J. P. *Eur. Cells Mater.* **2002**, *3*, 102−105.

(9) Stevenson, J. P.; Rutnakornpituk, M.; Vadala, M. L.; Esker, A. R.; Charles, S. W.; Wells, S.; Dailey, J. P.; Riffle, J. S. *J. Magn. Magn. Mater.* **2001**, *225*, 47−58.

(10) Vadala, M. L.; Zalich, M. A.; Fulks, D. B.; St. Pierre, T. G.; Dailey, J. P.; Riffle, J. S. *J. Magn. Magn. Mater.* **2005**, *293*, 162−170.

(11) Wilson, K. S.; Goff, J. D.; Riffle, J. S.; Harris, L. A.; St. Pierre, T. G. *Polym. Adv. Technol.* **2005**, *16* (2−3), 200−211.

(12) Kim, D. K.; Mikhaylova, M.; Zhang, Y.; Muhammed, M. *Chem. Mater.* **2003**, *15* (8), 1617−1627.

(13) Si, S.; Kotal, A.; Mandal, T. K.; Giri, S.; Nakamura, H.; Kohara, T. *Chem. Mater.* **2004**, *16*, 3489−3496.

(14) Lutz, J.-F.; Stiller, S.; Hoth, A.; Kaufner, L.; Pison, U.; Cartier, R. *Biomacromolecules* **2006**, *7*, 3132−3138.

(15) Wormuth, K. *J. Colloid Interface Sci.* **2001**, *241*, 366−377.

(16) Molday, R. S. U.S. Patent 4452773, 1984.

(17) Suzuki, M.; Shinkai, M.; Kamihira, M.; Kobayashi, T. *Biotechnol. Appl. Biochem.* **1995**, *21*, 335−345.

(18) Harris, L. A.; Goff, J. D.; Carmichael, A. Y.; Riffle, J. S.; Harburn, J. J.; St. Pierre, T. G.; Saunders, M. *Chem. Mater.* **2003**, *15* (6), 1367−1377.

(19) Noguchi, H.; Yanase, N.; Uchida, Y.; Suzuta, T. *J. Appl. Polym. Sci.* **1993**, *48* (9), 1539−1547.

(20) Hunter, R. J., *Foundations of Colloid Science;* Clarendon Press: Oxford, UK, 1992.

(21) Verwey, E. J. W.; Overbeek, J. T. G. *Theory of the Stability of Lyophobic Colloids*; Dover: Mineola, NY, 2000.

(22) Deryaguin, B. V.; Landau, L. D. *Acta Physicochim. (USSR)* **1941**, *14*, 633−652.

(23) Verwey, E. J. W.; Overbeek, J. T. G. *Theory of the Stability of Lyophobic Colloids*; Elsevier: Amsterdam, 1948.

10.1021/la703146y CCC: $40.75
Published on Web 03/27/2008

a means for predicting the net interaction energy including van der Waals, electrostatic, and steric forces in dilute dispersions. By varying the factors that contribute to each of the forces, the net interactions of particles can be controlled, leading to control over colloid stability and flocculation rates. For instance, the rate at which gold nanoparticles agglomerate has been altered by changing the electrostatic charge on the surface of the particles[20] or alternatively by changing the ionic properties of the medium.[24,25] The stabilities of magnetic nanoparticle dispersions have also been investigated by altering the pH in the presence of applied external magnetic fields. This altered the electrostatic repulsions and resulted in flocculation of magnetite particles in strong magnetic fields.[26] It has also been observed that magnetic nanoparticles can form chainlike structures in dilute dispersions with application of an applied field.[27]

This paper will describe the size distribution of PDMS−magnetite nanoparticle complexes, where the PDMS forms a stabilizing brush layer that contributes significantly to the overall size of the complexes. For a given slice in the size distribution, the DLVO theory can provide qualitative insight into the stability against flocculation, an important issue for applications of these complexes. In this work, dilute suspensions of the polymer−nanoparticle complexes are considered in both a good solvent for the PDMS and a theta solvent and the viscosities of an undiluted fluid will be presented.

Experimental

Materials. Hexamethylcyclotrisiloxane (D_3, Gelest, 98%) was dried over calcium hydride and sublimed under vacuum into preweighed, flame-dried, round-bottom flasks, each containing a magnetic stir bar. The flasks were purged with nitrogen and reweighed to determine the amount of D_3 in each flask. Cyclohexane (EM Science, 99%) was stirred with concentrated sulfuric acid for 48 h, washed with deionized water until neutral, stirred over magnesium sulfate, then over calcium hydride, distilled, stored over sodium under a nitrogen atmosphere, and redistilled prior to use. Tetrahydrofuran (THF, EM Science, 99.5%) was dried over calcium hydride, distilled, and stored over sodium in the presence of benzophenone under a nitrogen atmosphere until the solution was deep purple in color. The THF was redistilled just prior to use. Toluene (Burdick and Jackson, 99.9%) was washed twice with concentrated sulfuric acid and neutralized with water. It was dried over magnesium sulfate for 1 h, then over calcium hydride overnight, and distilled just before use. Aqueous hydrochloric acid (50% by volume) was prepared by adding 5 mL of concentrated hydrochloric acid (EM Science) to 5 mL of deionized water in a graduated cylinder. Ferric chloride hexahydrate ($FeCl_3 \cdot 6H_2O$) and ferrous chloride tetrahydrate ($FeCl_2 \cdot 4H_2O$) (both from Aldrich) were stored under nitrogen in a desiccator and used as received. Iron granules (Alfa Aesar, 1−2 mm, 99.98%) were washed repeatedly with a variety of solvents to remove any coating on the surface. The granules were subsequently dried overnight in a vacuum oven at 40 °C. Ammonium hydroxide (Alfa Aesar, 50%, v/v, aqueous), mercaptoacetic acid (Aldrich, 97%), 2,2′-azobisisobutyronitrile (AIBN, 98%, Aldrich), *n*-butyllithium (1.6 M, Aldrich), trivinylchlorosilane (Gelest, 95%), octamethylcyclotetrasiloxane (D_4, 99%, Gelest), and trimethylchlorosilane (Gelest, 99%) were used as received. NdFeB doughnut-shaped magnets that were magnetized through the thickness were purchased from Engineered Concepts. The field generated by the doughnut magnets was 0.24 T, and the magnets had dimensions of 0.5 in (1.27 cm) i.d., 1.0 in (2.54 cm) o.d., and 0.25 in (0.635 cm) thickness.

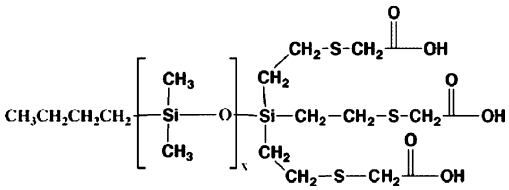

Figure 1. Tricarboxylic acid functional PDMS.

Synthesis of PDMS-Coated Magnetite Nanoparticles. The method for synthesizing the nanoparticles complexed with a carboxylate-functional PDMS (Figure 1) has been previously reported.[7,11] The PDMS oligomer that was utilized for the ferrofluid in the present work was 3242 g mol^{-1}. The PDMS dispersion stabilizer was prepared by the following method.

D_3 (51.23 g, 0.23 mol) was sublimed into a flame-dried, round-bottom flask. The flask was purged with nitrogen, and cyclohexane (50 mL) was added to the flask via a syringe. Once the D_3 monomer dissolved at room temperature, 1.6 M *n*-butyllithium (10.86 mL, 0.0174 mol) was added to the reaction flask, and the solution was stirred for 0.5 h. THF (15 mL) was then charged to the solution as a reaction promoter. ^{1}H NMR was used to monitor the progress of the living anionic polymerization. At ∼95% conversion of monomer, the polymer was terminated with an excess of trivinylchlorosilane (3.78 mL, 0.0261 mol), and the mixture was stirred overnight. The PDMS oligomer was diluted with chloroform and washed with deionized water (3×). The solution was concentrated under vacuum and poured into methanol to precipitate the liquid polymer. The polymer was dried under vacuum at 80 °C overnight.

A thiol-ene addition of mercaptoacetic acid to the trivinylsilane-functional PDMS oligomer was conducted as follows. A 2800 g mol^{-1} trivinylsiloxy terminated PDMS (15 g, 0.016 eq vinyl) was added into a flame-dried, round-bottom flask and dissolved in distilled toluene (25 mL). The reaction solution was deoxygenated by sparging with nitrogen through the solution for 2 h. AIBN (0.0037 g, 2.4 × 10^{-4} mol) and mercaptoacetic acid (1.67 mL, 0.024 mol) were added to the reaction vessel, and the flask was purged with nitrogen. The reaction was heated to 80 °C and stirred for 1 h. Reaction completion was confirmed by observing the disappearance of the vinyl proton peaks at ∼6 ppm in the ^{1}H NMR spectra. The solvent was removed under vacuum, and the polymer was dissolved in methanol (30 mL) by stirring for 30 min. Deionized water was added to the solution until the polymer coagulated as a solid, and then it was collected via filtration. The methanol/deionized water coagulation process was repeated five times, then the polymer was dried under vacuum at 80 °C. The M_n of the functionalized PDMS oligomer was determined to be 3242 g mol^{-1} by ^{1}H NMR. Size Exclusion Chromatography (SEC) analysis determined the number average molecular weight to be 3393 g mol^{-1} with a polydispersity index of 1.15.

The preparative method for a 70:30 by weight PDMS stabilizer: magnetite complex is provided. Magnetite was synthesized by the chemical precipitation of iron salts. Iron(III) chloride hexahydrate (2.01 g, 0.00744 mol) and iron(II) chloride tetrahydrate (0.736 g, 0.00370 mol) were weighed into separate round-bottom flasks, and each was dissolved in 20 mL of deoxygenated water. The two iron salt solutions were charged to a 500 mL, three-necked round-bottom flask equipped with an UltraTurrax T25 homogenizer. Careful attention was paid to maintain an oxygen-free environment by purging the reaction vessel with a heavy flow of nitrogen. The homogenizer speed was set to 13 000 rpm, and ammonium hydroxide (15 mL) was added via a syringe until the homogenizing solution turned black and reached a pH of 9−10. The 3242 g mol^{-1} PDMS dispersion stabilizer (2.0 g) was dissolved in dichloromethane (60 mL) and was added to the basic magnetite dispersion. The mixture was stirred for approximately 30 min and 50 vol % aqueous hydrochloric acid (∼6 mL) was added slowly until the solution became slightly acidic (pH 5−6). The acidic interfacial solution was stirred for ∼1 h, and then the dichloromethane was removed under vacuum. The magnetite complex was collected with a magnet and the water was decanted.

(24) Kim, T.; Lee, K.; Gong, M.-S.; Joo, S.-W. *Langmuir* **2005**, *21*, 9524−9528.
(25) Viudez, A. J.; Madueno, R.; Pineda, T.; Blazquez, M. *J. Phys. Chem. B* **2006**, *110*, 17840−17847.
(26) Tsouris, C.; Scott, T. C. *J. Colloid Interface Sci.* **1995**, *171*, 319−330.
(27) Pshenichnikov, A. F.; Fedorenko, A. A., *J. Magn. Magn. Mater*. **2005**, *292*, 332−344.

The magnetite complex was washed several times with water (5×) and methanol (5×) before drying overnight at 40 °C under reduced pressure.

Magnetic separation columns comprised of ∼6 g of soft iron granules were firmly packed in 3 mL plastic syringes. A magnetic field was generated by a 0.24 T NdFeB doughnut-shaped magnet placed around the exterior of the syringe. The PDMS−magnetite nanoparticles were diluted in chloroform (chloroform is a good solvent for PDMS[28]) to a concentration of 0.002 mg mL^{-1}. The dispersion was sonicated with a Biologics ultrasonic homogenizer (model 150V/T) for 5 min using the 50% power setting with a microtip probe and a 50% pulse. Following sonication, 150 mL of the chloroform dispersion (0.3 g of particles) was passed through the column at a flow rate of ∼20 mL min^{-1} and collected.

Characterization. Thermogravimetric analysis (TGA) was carried out on the PDMS−magnetite nanoparticles using a TA Instruments TGA Q500 instrument. After equilibrating the samples at 25 °C, the temperature was ramped at 10 °C min^{-1} to a maximum temperature of 650 °C under a nitrogen purge. Char yields (the mass remaining at the end of the experiment) were recorded at the maximum temperature.

Elemental analysis via inductively coupled plasma sector field mass spectrometry (ICP-MS) was conducted with a Thermo Finnigan Element 2 ICP-MS instrument equipped with a PFA Teflon double pass (Scott type) spray chamber with a Teflon concentric nebulizer (operating at ∼1 mL min^{-1} flow of argon and the sample flow was 1 mL min^{-1}). Samples of Fe (*m*/*z* 54, 56, and 57) and Si (*m*/*z* 28 and 29) were analyzed and the concentrations of the isotopes were averaged (3 replicates, 10 reads per replicate). All were measured at medium resolution ($R = 4000$). Samples were digested in a 1:1 HNO_3:H_2SO_4 mixture prior to measurement.

SEC was obtained in chloroform at 30 °C on a Waters Alliance Model 2690 chromatograph equipped with a Waters HR 0.5 + HR 2 + HR 3 + HR 4 styragel column set. A Viscotek viscosity detector and a refractive index detector were utilized with polystyrene calibration standards to generate a universal molecular weight calibration curve for absolute molecular weight analyses.

Transmission electron microscopy (TEM) was conducted with a JEOL 3000F field-emission-gun transmission electron microscope (operated at 300 kV) equipped with a 1024 × 1024 pixel digital imaging system. Dry samples of the magnetite complexes were dispersed in chloroform and cast onto amorphous carbon-coated copper grids for analysis. Great care was taken to ensure that both eucentric height and focus were set consistently from one sample to another in order to reduce uncertainty in the digital image analysis. Images were acquired at a magnification of 300 k× corresponding to 1.65 pixels nm^{-1}. This magnification yielded both sufficient resolution and contrast for digital image analysis and provided a large enough field of view to measure adequate numbers of particles. Particle size analysis was performed using Reindeer Graphics' Fovea Pro 4 plug-in for Adobe Photoshop CS2. Means and standard deviations of the particle size diameters were calculated based upon 3500−5000 particles per sample, and particle size distributions were fitted with a Weibull distribution.

Dynamic light scattering (DLS) measurements were conducted with a Malvern Zetasizer ZS compact scattering spectrometer (Malvern Instruments Ltd, Malvern, UK) at a wavelength of 633 nm from a 4.0 mW, solid-state He−Ne laser at a scattering angle of 170°. Intensity average, volume average, and number average diameters were calculated from the autocorrelation function using Malvern's Zetasizer Nano 4.2 software utilizing a version of the CONTIN algorithm.[29]

Rheology measurements were conducted with a TA Instruments AR-G2 rheometer equipped with a stainless steel cone with an angle of 0.5° and a diameter of 20 mm (truncation 12 μm). The sample volume was approximately 0.03 mL. Steady-state flow experiments were conducted measuring the viscosity of the neat complexes at shear rates from 0.00001 to 10 000 s^{-1} at 25 °C with no preshearing protocol. For comparison, a sample aged for 30 days was then presheared at 10 000 s^{-1} for 2 min before measurements were made.

Results and Discussion

Synthesis and Separation of PDMS−Magnetite Complexes. Magnetite nanoparticles were prepared by reacting a stoichiometric ratio of $FeCl_2$ and $FeCl_3$ with hydroxide ion in an oxygen-free environment while being mixed rapidly by a homogenizer. The homogenizer was employed in efforts to minimize aggregate formation during the nanoparticle precipitation process. The surfaces of the magnetite nanoparticles were subsequently coated by adsorbing a PDMS oligomer that had three carboxylates on one end and a nonfunctional trimethylsilyl group at the other (Figure 1). The M_n of the functionalized PDMS oligomer was determined to be 3242 g mol^{-1} by ^1H NMR. After a thorough washing procedure to remove any unbound polymer, a chloroform dispersion of the PDMS−magnetite complexes was passed through a magnetic separation column to remove any large particles and aggregates that might have formed during synthesis.[30] The particle−polymer composition ratios were determined by weight loss measurements (TGA). The amount of polymer on the surface of the magnetite must be known to calculate the thickness of the stabilizing layer that prevents particle aggregation. The materials were heated under nitrogen in the TGA furnace past the point of thermal degradation of the PDMS brushes, and this left only the magnetite mass as a residual char. As previously reported, the PDMS oligomer leaves no detectable char above 650 °C when heated under these conditions.[31] It has also been previously demonstrated that the magnetite does not lose any weight under these conditions.[32] The resulting nanoparticle complex was determined by TGA to contain 30 wt % of magnetite and 70 wt % of PDMS oligomer, as targeted. The atomic ratio of Si/Fe for the polymer−nanoparticle complex was 2.30. Elemental analysis by ICP-MS of the complex following pyrolysis in the TGA determined the atomic ratio of Si/Fe to be 0.018. This indicates that almost all the PDMS was removed during the TGA measurement.

Sizes and Size Distributions of the Magnetite Nanoparticles. Particles produced via coprecipitation of iron salts as described herein are polydisperse in size. Therefore, to understand the interactions among this distribution of particles, a necessary first step is to characterize the particle size and size distribution. TEM in conjunction with image analysis is an effective means to measure the core particle sizes. A chloroform dispersion of the PDMS−magnetite complex was cast onto a carbon-coated TEM grid, and the chloroform was allowed to evaporate at room temperature. This sample preparation protocol resulted in the nanoparticles being fairly evenly spread across the grid. Images of the particles were taken at 300 000 times magnification (Figure 2), since this offered the best contrast of particles to background at acceptable resolution.

Size analyses were carried out to determine the distribution of the diameters of the magnetite cores of the nanoparticles. Seven TEM images of the sample were analyzed, resulting in 8439 particles being measured. The images were blurred slightly (2 pixels) to flatten noise in the background, and then an intensity

(28) Lee, J. N.; Park, C.; Whitesides, G. M. *Anal. Chem.* **2003**, *75*, 6544−6554.

(29) *Calculating Volume Distribution From Dynamic Light Scattering. Frequently Asked Questions*; Malvern Instruments: Worcestershire, UK, 2007.

(30) Mefford, O. T.; Carroll, M. R. J.; Vadala, M. L.; Goff, J. D.; Mejia-Ariza, R.; Saunders, M.; Woodward, R. C.; St. Pierre, T. G.; Davis, R. M.; Riffle, J. S. *Chem. Mater.* **2008**, in press.

(31) Jovanovic, J. D.; Govedarica, M. N.; Dvornic, P. R.; Popovic, I. G. *Polym. Degrad. Stab.* **1997**, *61*, 87−93.

(32) Zhang, Q.; Thompson, M. S.; Carmichael, A. Y.; Caba, B. L.; Zalic, M. A.; Lin, Y. N.; Mefford, O. T.; Davis, R. M.; Riffle, J. S. *Langmuir* **2007**, *23*, 6927−6936.

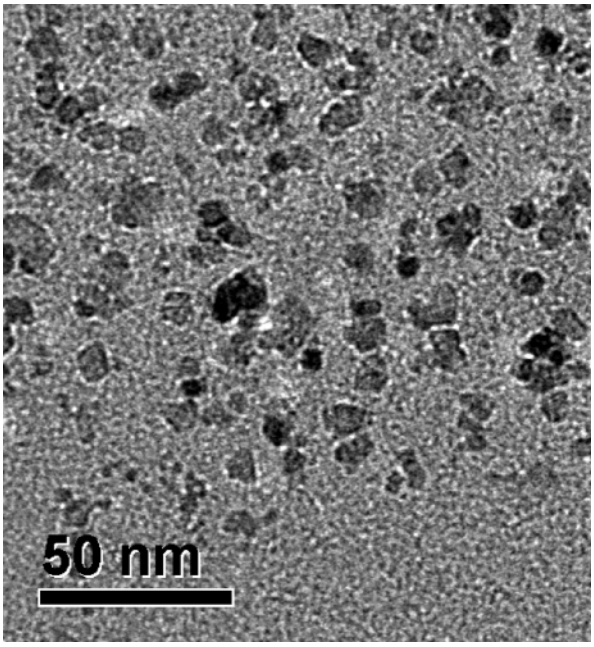

Figure 2. Representative TEM image of PDMS−magnetite particles.

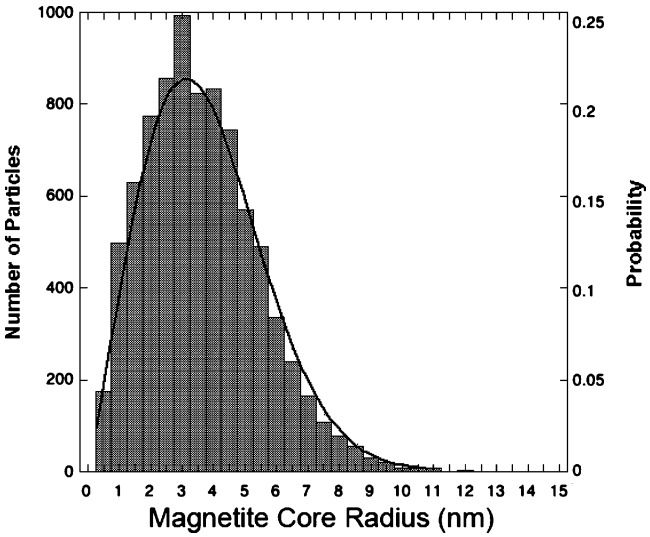

Figure 3. Histogram of the radii of the magnetite cores fitted with a Weibull probability function.

threshold was applied to distinguish the particles from the background. Fovea Pro's watershed tool was utilized to distinguish particles that were close together but not connected. The original image was compared to the threshold image (the image that the software interpreted to be particles) to check for any discrepancies, and all of the detected errors were manually corrected on the threshold image before particle sizes were measured. This ensured that only true particles were identified in the images and any potential artifacts were removed prior to analysis. The arithmetic mean and standard deviation of core diameters in the distribution were calculated to be 7.2 and 3.6 nm respectively. It was found that the particle size distribution could be accurately represented ($R^2 = 0.996$) by a two-parameter Weibull distribution (Figure 3).

$$P(r) = \frac{\gamma}{\alpha}\left(\frac{r}{\alpha}\right)^{\gamma-1}\exp\left(\frac{-r}{\alpha}\right)^{\gamma} \qquad (1)$$

where $P(r)$ is the probability of a particle with radius r, α is a scale parameter ($\alpha = 4.07$ nm), and γ is a shape parameter ($\gamma = 2.11$).

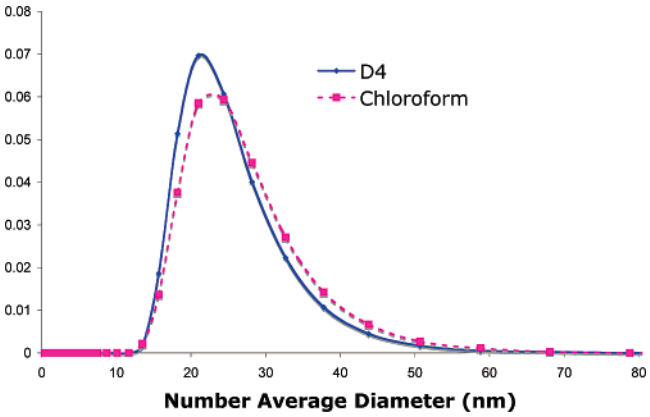

Figure 4. Number average diameters of the PDMS−Magnetite complex in D_4 and chloroform suspensions from DLS.

Table 1. Calculated and Measured Values of the Intensity, Volume, and Number Averages of the PDMS−Magnetite Complex Diameter from Eqs 14, 15, and 22

	calculated diameter (TEM)		measured hydrodynamic diameter D_h (DLS)	
solvent	good	theta	$CHCl_3$	D_4
intensity average	24.4	23.4	41.2 ± 0.4	46.8 ± 0.6
volume average	22.4	21.2	30.2 ± 0.6	32.7 ± 1.9
number average	18.7	17.0	24.0 ± 0.8	25.4 ± 2.4

Solution Sizes of the PDMS−Magnetite Nanoparticles. The PDMS−magnetite complex was dispersed in either chloroform or D_4. Chloroform has been shown to be a good solvent for PDMS,[28] and because the repeat unit for D_4 and PDMS is the same, it was reasoned that dispersions in D_4 would approximate theta conditions. There was little if any effect of the solvent quality on the averages (intensity, volume, and number averages) of the hydrodynamic diameter D_h measured by DLS of the particles in the two solvents (Figure 4 and Table 1). This is reasonable considering the end-to-end distance of an unperturbed PDMS chain of 3242 g mol^{-1} in solution (3.1 nm for a theta solvent from the wormlike chain model)[33] and its contour length (12.6 nm) relative to the calculated brush thickness (mean is 6.4 nm). The high surface chain density of 3.9 chains nm^{-2} (21 mg m^{-2}) results in highly stretched PDMS corona chains even in theta conditions. Thus, changing the solvent quality from a theta to a good solvent results in little change in the layer thickness. This is borne out by the calculated values of the average diameters based on the brush model (see eqs 13, 14, and 21 below). The averages in both solvents vary in the expected order: intensity > volume > number. In addition, the shape of the distribution of particles was very similar to that of the core particle sizes, indicating that it might be possible to calculate the size of the total complex based on the measured core particle sizes.

Calculations of Particle−Particle Interactions. A modified form of DLVO theory was utilized to examine interparticle energies to predict stabilities of dilute dispersions of these complexes. The particle−particle interaction potentials were calculated by summing the potentials of van der Waals, V_a, and magnetic, V_m, attractions along with electrostatic, V_e, and steric, V_s, repulsions (eq 2).

$$V_{total} = V_a + V_e + V_s + V_m \qquad (2)$$

The potentials were normalized by thermal energy, k_BT, where k_B is Boltzmann's constant and T is temperature in Kelvin.

(33) Yamakawa, H. *Modern Theory of Polymer Solutions*; Harper and Row: New York, 1971.

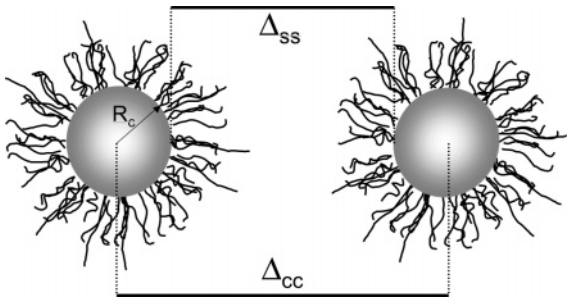

Figure 5. Schematic illustrating distances between particles: center-to-center distance, Δ_{cc}, and surface-to-surface separation of magnetite cores, Δ_{ss}.

Normalizing the data to thermal energy allows for inferences to be made regarding the relative energetics of energy wells that exist with certain compositions, thus suggesting that agglomeration would be likely present. In addition, the potentials were calculated as functions of the radii of the magnetite cores, R_c, derived from the TEM size analyses. By considering the net potential as a function of the radius of the magnetite, predictions for the stabilities of dispersions were made for discrete points along the distribution of core particle sizes.

The van der Waals portion of the total interaction potential, V_a, was calculated as a function of the magnetite surface-to-surface distance, Δ_{ss}, between two particles of equal size having a core radius, R_c (eq 3 and Figure 5).[34,35] where k_B is Boltzmann's

$$V_a = -\frac{1}{6k_BT}A_{eff}\left(\frac{2R_c^2}{\Delta_{ss}(4R_c+\Delta_{ss})}+\frac{2R_c^2}{(2R_c+\Delta_{ss})^2}+\ln\left(\frac{\Delta_{ss}(4R_c+\Delta_{ss})}{(2R_c+\Delta_{ss})^2}\right)\right) \quad (3)$$

constant (1.38×10^{-23} J K^{-1}), T is the temperature (298 K), and A_{eff} is the effective Hamaker constant that includes retardation effects. A_{eff} was derived from eq 4. where $\epsilon(0)$ and $\bar{\epsilon}(0)$ are the

$$A_{eff} = \frac{3}{4}k_BT\left(\frac{\bar{\epsilon}(0)-\epsilon(0)}{\bar{\epsilon}(0)+\epsilon(0)}\right)^2+\frac{3h\omega}{16\sqrt{2}}\frac{(\bar{n}_0^2-n_0^2)^2}{(\bar{n}_0^2+n_0^2)^{3/2}}F(\delta) \quad (4)$$

dielectric constants for the medium (PDMS) and the substrate (magnetite) (2.5[36] and 20 000,[32] respectively), n_0 and $\bar{n_0}$ are the low-frequency refractive indices of the medium and substrate (1.43[36] and 1.970,[32] respectively), $\hbar$ is Planck's constant (6.63×10^{-34} J s), and ω is the frequency of the dominant relaxation in the UV (1.88×10^{16} rad s^{-1}). The function $F(\delta)$ accounts for retardation effects and approaches unity at the point of surface-to-surface contact.

$$F(\delta) \approx \left(1+\left(\frac{\pi\delta}{4\sqrt{2}}\right)^{3/2}\right)^{-2/3} \quad (5)$$

where δ is a dimensionless surface-to-surface distance relative to the dimensional surface-to-surface separation, Δ_{ss}.

$$\delta = n_0(\bar{n}_0^2+n_0^2)^{1/2}\frac{\Delta_{ss}\omega}{c} \quad (6)$$

where c is the speed of light (3×10^8 m s^{-1}).

The electrostatic component for the particle−particle potential was calculated via eq 7, where ϵ_0 is the permittivity of free space,

$$V_e = \frac{2\pi R_c\epsilon(0)\epsilon_o\psi_o^2\ln(1+e^{-\kappa\Delta ss})}{k_BT} \quad (7)$$

Ψ_0 is the surface potential, and $1/\kappa$ is the Debye length. The surface potential of magnetite synthesized by the method described herein has been reported to be ~1.3 mV at neutral pH.[32] Because PDMS is extremely nonpolar, there is only a very low concentration of electrolytes, and this results in the Debye length, $1/\kappa$, approaching zero.[34,37] Thus eq 7 reduces to $V_e \approx 0$.

The steric potential relies strongly on the number of chains on each particle. Because the number of chains per particle is directly related to the radius of the magnetite core, R_c, the steric interaction potential was calculated as a function of the core particle size.

The average chain density, $\bar{\sigma}$ (the number of chains per nm^2 of magnetite surface), was calculated using the Weibull probability functions of the magnetite core sizes from TEM image analysis, and compositions of the complexes were obtained from TGA according to

$$\bar{\sigma} = \frac{W_{PDMS}N_{Av}\rho_{mag}}{M_nW_{mag}}\int_0^\infty\left(\frac{3}{r}\right)P(r)\,dr \quad (8)$$

where W_{PDMS} and W_{mag} are the mass fractions of the complex that consists of PDMS and magnetite, respectively, ρ_{mag} is the density of magnetite (5.17 g mL^{-1}),[38] M_n is the number average molecular weight of the PDMS chains, and N_{Av} is Avogadro's number. The ratio ($3/r$) in the integral arises from the area/volume ratio for a sphere. The average functionality (number of chains per particle), $f(r)$, of a particle of given radius is then

$$f(r) = 4\pi r^2\bar{\sigma} \quad (9)$$

Polymer Brush Size and Chain Density on the Magnetite Surface. A promising model for our polymer−magnetite complexes is the density distribution (DD) model developed by Vagberg et al.[39] On the basis of a model for star polymers by Daoud and Cotton,[40] the DD model assumes concentric shells with a constant number of blobs in each shell (Figure 6). The blob diameter, ξ(r), is a continuous function of distance from the surface. The segment density in the shell varies with distance from the core that, in the present case, is the surface of the magnetite particle. In the present case, this model is an improvement over flat surface models that have been utilized for predicting steric interactions. By accounting for effects of surface curvature and changes in chain density in determining the brush thickness, the physics of chain interpenetrations can be better described.

The DD model predicts the radius, R_m, of the PDMS−magnetite complex.

(34) Israelachvili, J. N. *Intermolecular and Surface Forces*; Academic Press: London, 1991.
(35) Stokes, R. J.; Evans, D. F. *Fundamentals of Interfacial Engineering*; Wiley-VCH: New York, 1996.
(36) Gelest, Silicon, Germanium, Tin and Metal-Organic Compounds in their 2006 catalog.
(37) Israelachvili, J. N. *Intermolecular and Surface Forces*; Academic Press: Orlando, FL, 1985.
(38) *CRC Handbook of Chemistry and Physics*, 87th ed.; Boca Raton, FL, 2006−2007.
(39) Vagberg, L. J. M.; Cogan, K. A.; Gast, A. P. *Macromolecules* **1991**, *24*, 1670−1677.
(40) Daoud, M.; Cotton, J. P. *J. Phys.* **1982**, *43(3)*, 531−538.

$$R_m(r) = \left(\frac{8N_k f(r)^{(1-\nu/2\nu)}}{3*4^{1/\nu}\nu} L_k^{1/\nu} + r^{1/\nu} \right)^{\nu} \quad (10)$$

where N_k is the number of statistical or Kuhn segments in one of the corona chains (a PDMS chain in the present case), ν is the Flory exponent, r is the radius of the magnetite core, and $f(r)$ is the number of corona chains per particle. For this work, the Flory exponent, ν, was varied between 0.5 for the case with D_4 as the dispersing medium to simulate theta conditions, to 0.6 for chloroform (a good solvent for PDMS). The statistical segment or Kuhn length L_k is defined as

$$L_k = c_\infty l_0 \quad (11)$$

and the number of statistical segments in a chain, N_k, is defined as

$$N_k = n/c_\infty \quad (12)$$

where c_∞ is the characteristic ratio (5.2 for PDMS[39]), l_0 is the average length of a backbone bond (0.155 nm for PDMS), and n is the number of backbone bonds in a chain (2 × degree of polymerization for the PDMS).

Calculation of Sizes of the PDMS−Magnetite Complexes. The number average diameter, $\overline{D_n}$, of the complex can be calculated as

$$\overline{D_n} = 2\int_0^\infty P(r)R_m(r)\,dr \quad (13)$$

The volume average diameter, $\overline{D_v}$, can be calculated as

$$\overline{D_v} = 2\left(\frac{3}{4\pi}\bar{V}_m\right)^{1/3} \quad (14)$$

where the average volume of the PDMS−magnetite nanoparticle complex, $\overline{V_m}$, is found by

$$\overline{V_m} = \frac{4}{3}\pi\int_0^\infty P(r)R_m^3(r)\,dr \quad (15)$$

The intensity average diameter was determined using a method developed by Prudhomme et al.[41] In dynamic light scattering, the particle sizes can be determined by first describing the relationship between the first cumulant, $\Gamma(q)$, and the scattering from a distribution of particles

$$\frac{\Gamma(q)}{q^2} = \frac{\sum_{j=1}^{\infty} n_j I_j D_j}{\sum_{j=1}^{\infty} n_j I_j} \quad (16)$$

where q is the wave vector, n_j is the number of particles at a particular radius r_j, I_j is the scattering intensity from these particles, and D_j is the diffusion coefficient.[42] The diffusion coefficient, D_0, for the particles can be described in terms of the first cumulant and the Stokes−Einstein relation.

$$D_0 = \frac{\Gamma(q)}{q^2} = \frac{k_B T}{6\pi\mu r} \quad (17)$$

where k_B is Boltzmann's constant, T is temperature in Kelvin, and μ is the viscosity of the solvent. By the combination of eqs 16 and 17, the intensity average radius, $\overline{R_I}$, can described in terms of

$$\frac{6\pi\mu\overline{R_I}}{k_B T} = \frac{\sum_{j=1}^{\infty} n_j I_j}{\sum_{j=1}^{\infty} n_j I_j \frac{k_B T}{6\pi\mu R_j}} \quad (18)$$

The hydrodynamic radii of the particles were shown by DLS to be on the order of 30 nm. Therefore these particles should be in the Rayleigh scattering range in which the scattering intensity, I_j, can be described as

$$I_j = I_0 q^4 \cos^2\theta \left[\left(\frac{n_p}{n_s}\right)^2 - 1\right]^2 \frac{R_j^6}{9\beta^2} F_f(\theta) \quad (19)$$

where I_0 is the incident light intensity, θ is the scattering angle, n_p and n_s are the refractive indices of the particle and the solvent, respectively, β is the distance from the particle to the light detector, and $F_f(\theta)$ is the Rayleigh form factor.[43] The scattering intensity is directly related to the radii of the particles to the sixth power, and thus eq 19 reduces to

$$\overline{R_I} = \frac{\sum_{k=1}^{\infty} n_k R_k^6}{\sum_{k=1}^{\infty} n_k R_k^5} \quad (20)$$

For a particle size distribution described by a Weibull probability function, the discrete summations in eq 20 can be replaced by integrals to calculate the intensity average diameter, $\overline{D_I}$ as

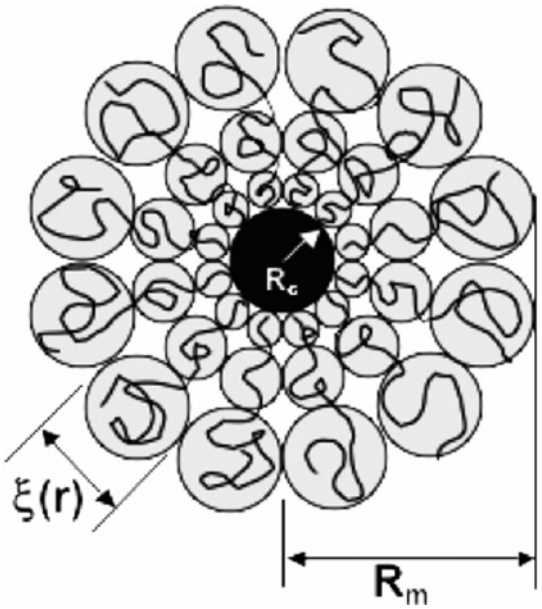

Figure 6. Representation of a PDMS−magnetite complex showing the model parameters, adapted from Daoud and Cotton.[40]

(41) Liu, Y.; Kathan, K.; Saad, W.; Prud'homme, R. K. *Phys. Rev. Lett.* **2007**, *98* (3), 036102/1−036102/4.

(42) Russel, W. B.; Saville, D. A.; Schowalter, W. R. *Colloid Dispersions*; Cambridge University: Cambridge, 1987.

(43) Fuller, G. G. *Optical Rheometry of Complex Fluids*; Oxford University Press: New York, 1995.

$$\overline{D_I} = 2\overline{R_I} = 2\frac{\int_0^\infty P(r)R_m(r)^6\,dr}{\int_0^\infty P(r)R_m(r)^5\,dr} \quad (21)$$

For a given quality of solvent (good, theta), the agreement between the calculated and measured values is best for the number averages (Table 1). This is reasonable since the number average in DLS measurements gives the least weight to the larger particles in the distribution. The effect of solvent quality on the sizes of the PDMS−magnetite complexes is accounted for in eq 15 and is found to be negligible, a trend that was also observed by DLS.

Radius of Gyration, R_g. A critical parameter for the steric interaction (eq 22) is the radius of gyration, R_g, of the particle-polymer complex. One approach is to experimentally measure this using a scattering technique such as static light scattering (SLS) or small angle neutron scattering (SANS). Alternatively, one can approximate R_g using the moment of inertia, I, and the mass, m, of a complex.

$$R_g = \sqrt{\frac{I}{m}} \quad (22)$$

The moment of inertia of a composite body is the sum of the moments of inertia of the components. For the case of a magnetite core having a corona of extended PDMS chains, the moment of inertia can be described as

$$I_{total} = I_{magnetite} + I_{corona} \quad (23)$$

Correspondingly, the mass of the ensemble is

$$m_{total} = m_{magnetite} + m_{corona} \quad (24)$$

and the radius of gyration of the entire complex is

$$R_g = \sqrt{\frac{I_{total}}{m_{total}}} \quad (25)$$

The moment of inertia of a mass, m, rotated about an axis at a distance r is given by[44]

$$I = \int r^2\,dm \quad (26)$$

Extending this to the moment of inertia of a sphere with density ρ at a distance r from the origin yields

$$I = \int r^2\rho(r)4\pi r^2\,dr \quad (27)$$

One must define the density of the PDMS−magnetite complex as a function of distance from the center, r. For $r < R_c$, the density is the bulk density of magnetite, $\rho_{magnetite}$.

$$\rho(r) = \rho_{magnetite} \text{ for } r < R_c \quad (28)$$

For the PDMS corona, the density is defined by the density distribution model[39] as

$$\rho(r) = m_s A\left(\frac{r}{a_s}\right)^{1/\nu} r^{-3} \text{ for } R_c < r < R_m \quad (29)$$

in which m_s is the mass of a segment of PDMS, and the constant of proportionality, A, is determined by the relationship between

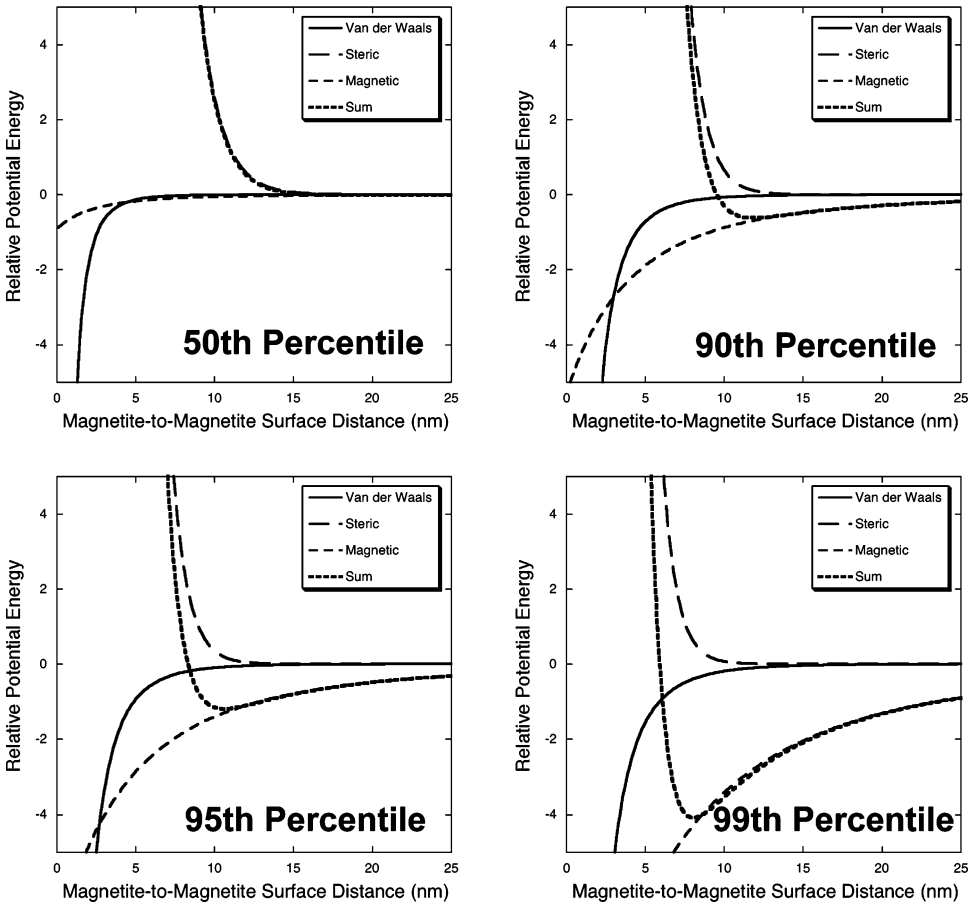

Figure 7. Relative potential energies calculated for two equal size particles at different percentiles of the distribution of magnetite core radii in theta solvent conditions. In the graph of the 50th percentile, it is noted that the V_s and the sum overlap.

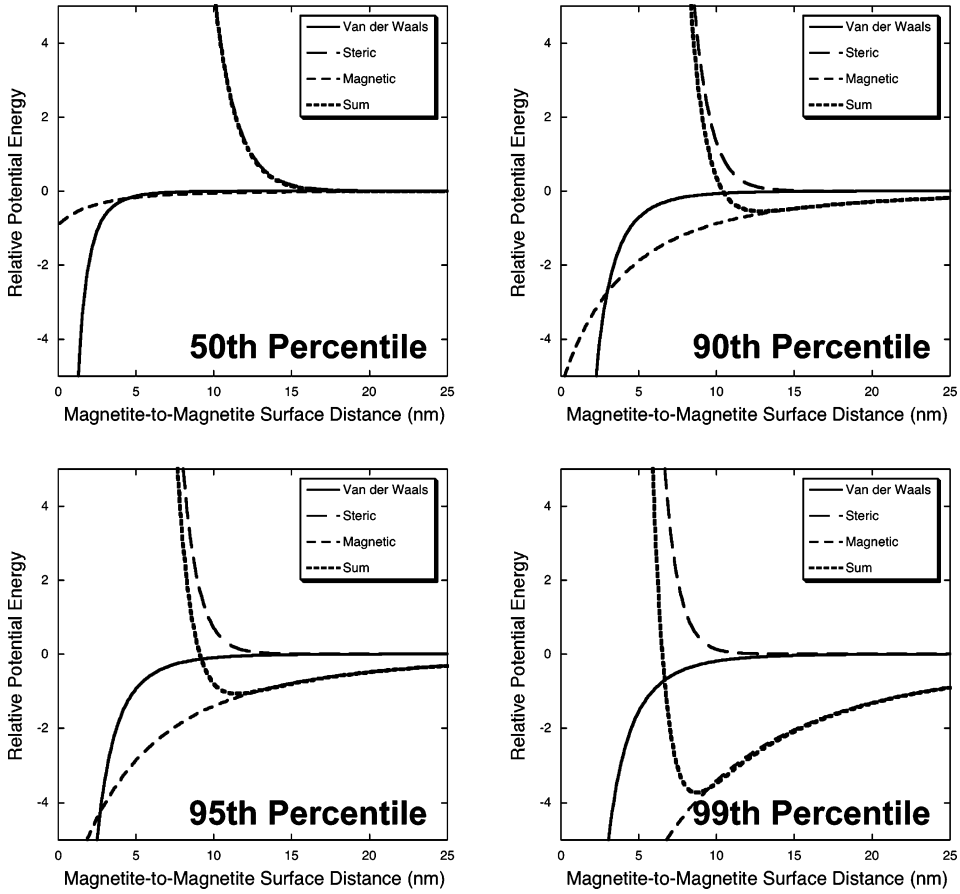

Figure 8. Relative potential energies calculated for two equal size particles at different percentiles of the distribution of magnetite core radii in good solvent conditions.

the blob size at the core−corona boundary and the number of corona chains, $f(R_c)$.

$$A = \frac{3 \times 4^{1/\nu} f(R_c)^{(3\nu-1/2\nu)}}{32} \tag{30}$$

Inserting the expressions in eq 28 and 29 into the formula for inertia given as eq 31 yields expressions for the inertia of the core and corona respectively.

$$I_{core} = \int_0^{R_c} r^2 \rho_{magnetite} 4\pi r^2 \, dr = \frac{4\pi {R_c}^5 \rho_{magnetite}}{5} \tag{31}$$

$$I_{corona} = \int_{R_c}^{R_m} r^2 m_s A\left(\frac{r}{a_s}\right)^{1/\nu} r^{-3} 4\pi r^2 \, dr = \frac{4\pi A m_s}{{a_s}^{1/\nu}\left(2+\frac{1}{\nu}\right)} ({R_m}^{(2+1/\nu)} - {R_c}^{(2+1/\nu)}) \tag{32}$$

The mass of the core and the corona can be calculated as:

$$m_{core} = \rho_{magnetite} \frac{4}{3} \pi {R_c}^3 \tag{33}$$

$$m_{corona} = f(R_c) \frac{M_n}{N_a} \tag{34}$$

Finally, having calculated R_g, the particle−particle steric interaction can be calculated as described by Likos et al.[45,46]

$$V_s = \begin{cases} \frac{5}{18} f(R_c)^{3/2}\left[-\ln\left(\frac{\Delta_{cc}}{\psi}\right) + \frac{1}{1+(\sqrt{f(R_c)}/2)}\right] & \text{for } \Delta_{cc} \le \psi \\ \frac{5}{18} f(R_c)^{3/2} \frac{1}{1+(\sqrt{f(R_c)}/2)} \left(\frac{\psi}{\Delta_{cc}}\right) \times \exp(\sqrt{f(R_c)}(\Delta_{cc}-\psi)/2\sigma) & \text{for } \Delta_{cc} \ge \psi \end{cases} \tag{35}$$

where ψ has been shown to scale in simulations as $\psi \cong 1.3R_g$.[47]

Calculations of Magnetic Interactions. The maximum magnetic interaction between two particles was calculated for the nanoparticles. It was assumed that all the particles were single domain particles and the spins for two interacting particles were aligned. This provides an upper bound for magnetic attractions between two particles in close proximity to one another. In this case, the interaction between the particles can be treated similarly to two magnetic dipoles.[48]

$$V_M = -\frac{1}{k_B T} \frac{8\pi\mu_0 {R_c}^6 {M_s}^2}{9(\Delta_{cc}+2R_c)^3} \tag{36}$$

(44) Beer, F. P.; Johnston, R. J. *Vector Mechanics for Engineers: Statics*; McGraw Hill: New York, 1990.

(45) Likos, C. N.; Lowen, H.; Watzlawek, M.; Abbas, B.; Jucknischke, O.; Allgaier, J.; Richter, D. *Phys. Rev. Lett.* **1998**, *80* (20), 4450−4453.

(46) Likos, C. N. *Soft Matter* **2006**, *2*, 478−498.

(47) Jusufi, A.; Watzlawk, M.; Lowen, H. *Macromolecules* **1999**, *32*, 4470−4473.

(48) Rosensweig, R. E. *Ferrohydrodynamics*; Cambridge University Press: New York, 1985.

Table 2. Particle Radii, Brush Thickness, Minimum Relative Potential Energy, and Distance at Minimum at Different Percentiles of the Size Distribution

	percentile							
	50th		90th		95th		99th	
solvent	theta	good	theta	good	theta	good	theta	good
particle radius (nm)	3.4		6.1		6.8		8.4	
brush thickness (nm)	6.2	7.2	7.4	7.7	7.6	7.9	8.0	8.2
complex radius (nm)	9.6	10.6	13.4	13.8	14.5	14.7	16.4	16.6
secondary min depth	−0.01	−0.01	−0.33	−0.32	−0.62	−0.63	−2.02	−2.04
separation distance at secondary min (nm)	23.9	23.7	17.5	17.6	16.4	16.4	14.5	14.4

where μ_0 is the permeability of free space (1.26×10^{-6} m kg s^{-2} A^{-2}), M_s is the saturation magnetization for magnetite (4.66×10^5A m^{-1}), and Δ_{cc} is the center-to-center distance of the particles.

Summing of Potentials for Different Points along the Magnetite Particle Size Distribution. Due to the polydisperse nature of the sizes of the magnetite cores, the interparticle potential cannot be simply calculated to represent the behavior of the entire sample. Population balance approaches have addressed the problem of interactions between particles of dissimilar sizes as the size distribution evolves with time from a monodisperse suspension.[49−51] However, the present system starts with a polydisperse distribution of magnetite core particles. While pair interaction models for binary colloids (i.e., two different sizes) exist for van der Waals, electrostatic, and magnetic effects, there is currently no such model for describing steric interactions. Thus, we employ the DLVO theory for particles in a given slice of the size distribution to gain qualitative insight into the effect of particle size on colloid stability.

Calculations of the net interaction potential were made at magnetite core sizes at the 50, 90, 95, and 99th percentiles of the size distribution. For instance, the 50th percentile is a radius in which 50% of the population of particles is smaller than 3.42 nm. Figures 7 and 8 illustrate the dimensionless potential energies calculated for van der Waals, electrostatic, steric, and magnetic interactions as well as the sum of the potentials for theta and good solvent conditions, respectively. As the size of the particle core increases, the total dimensionless potential energy develops a minimum (Table 2). The dispersion properties in terms of stability against flocculation for both cases are remarkably similar. The net potential is only weakly influenced by the solvent conditions, and particle size is the dominant factor. At larger particle sizes, the distance between the particles at the energy minimum closely approximates twice the length of the polymer brush on the surface of the magnetite. At the highest percentile considered (99th), the energy well is approximately twice that of thermal energy, a criterion for the onset of weak flocculation into a secondary minimum.[42] Agglomerates formed from this part of the size distribution would form effectively larger magnetic bodies, and these would have a larger dipole moment collectively. Moreover, the newly formed clusters could act as nucleation sites for further agglomeration, first capturing large particles and then smaller particles over time.

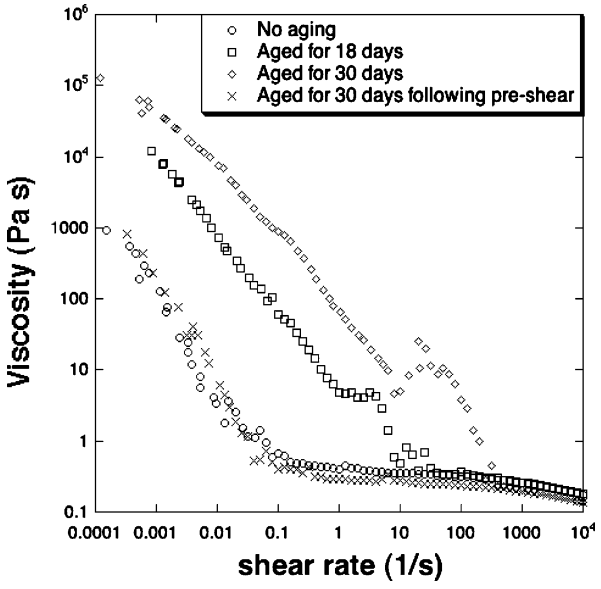

Figure 9. Rheological measurements of PDMS−magnetite nanoparticles over time.

Rheology of Neat Magnetite−PDMS Complex Fluids. While the suspension properties of these complexes are important in dilute media, their behavior as neat fluids is also of interest. One of the applications of these complexes is as ferrofluids for closing holes in retinal tissue.[6,7,9−11] In such cases, the complexes must be free of solvent and have flow properties suitable for clinical purposes. The fluid nature of these complexes even without addition of a dispersing medium or carrier fluid is a consequence of the mobile PDMS chains that are terminally bound to the magnetite cores at only one end. This property, in combination with the biocompatibility of the fluids, make these materials uniquely suited for their intended application of remotely closing retinal holes.[6−11] Fluids of functionalized metal oxide nanoparticles with similar liquidlike properties have also been synthesized by other authors.[52−54] For instance, silica nanoparticles have been functionalized with positively charged organosilanes. Salts were formed on the surface by the addition of either an isostearate or a sulfonate.[52]

To probe the stability of the PDMS−magnetite ferrofluids (without solvent), the rheological properties were investigated as a function of aging time for periods of up to 30 days (Figure 9). Viscosity (especially at low shear rates) increased as the samples were aged, suggesting that there might be some formation of clusters. To test if the nanoparticles were irreversibly clustered due to aging, a sample that had been aged for 30 days was sheared at 10 000 s^{-1} for 2 min and then the viscosity was remeasured. The viscosity of the sheared sample closely matched the sample that was not aged, suggesting that the clusters had been broken up.

(49) Chin, C.-J.; Yiacoumi, S.; Tsouris, C. *Langmuir* **2001**, *17*, 6065−6071.
(50) Chin, C.-J.; Yiacoumi, S.; Tsouris, C. *Colloids Surf.* **2002**, *204*, 63−72.
(51) Chin, C.-J.; Yiacoumi, S.; Tsouris, C.; Relle, S.; Grant, S. B. *Langmuir* **2000**, *16*, 3641−3650.
(52) Bourlinos, A. B.; Giannelis, E. P.; Zhang, Q.; Archer, L. A.; Floudas, G.; Fytas, G. *Eur. Phys. J. E* **2006**, *20*, 109−117.
(53) Warren, S. C.; Banholzer, M. J.; Slaughter, L. S.; Giannelis, E. P.; DiSalvo, F. J.; Wiesner, U. B. *J. Am. Chem. Soc.* **2006**, *128*, 12074−12075.
(54) Noginova, N.; Weaver, T.; King, M.; Bourlinos, A. B.; Giannelis, E. P.; Atsarkin, V. A. *J. Phys.: Condens. Matter* **2007**, *19* (7), 076210/1−076210/10.

Conclusions

Magnetite nanoparticles were synthesized by reacting iron salts with a base, and then a PDMS oligomer was adsorbed onto the magnetite nanoparticle surfaces. TEM was used in combination with a polymer brush model to calculate the size distribution of the PDMS−magnetite complexes. The net interparticle potentials for four different particle sizes, representing different portions of a magnetite core size distribution, were examined to obtain a better understanding of the effect of particle size on the overall stability of dispersions against flocculation. It was observed that larger particles induced an energy well at a magnetite surface-to-surface distance approximately twice that of the polymer brush. For 1% of the particles in the system, the energy well was greater than $2k_BT$, indicating that some agglomeration may occur in dispersions of these polymer−magnetite nanoparticles over time. Finally, the effect of aging on the shear viscosity of a magnetite−PDMS ferrofluid was probed via rheological measurements over time. Increases in shear viscosity (especially at low shear) suggested that some clustering occurs. These clusters could, however, be broken up by applying shear.

Acknowledgment. The authors are grateful for the financial support of the NSF/ARC Materials World Network for the Study of Macromolecular Ferrofluids (DMR-0602932 and LX0668968), the National Eye Institute of the NIH under SBIR contract B6867G1, and the ARC Discovery Grant-DP0559333. Transmission electron microscopy was carried out using the facilities at the Centre for Microscopy, Characterisation and Analysis, The University of Western Australia, which is supported by University, State, and Federal Government funding.

LA703146Y